JOURNAL OF AIRCRAFT
Vol. 39, No. 6, November–December 2002

Hingeless Flow Control over a Delta-Wing Planform

E. B. Moeller* and O. K. Rediniotis†
Texas A&M University, College Station, Texas 77843-3141

An experimental investigation of hingeless flow control by vortex breakdown manipulation over a delta wing is described. Employed as a method of longitudinal control for slender-wing planforms, the performance of this active flow control technique was evaluated as a possible replacement to conventional moving or hinged control surfaces. Testing was conducted with a 60-deg delta-wing model incorporating pneumatic vortex control (PVC) actuators. These actuators delivered high-pressure jets of varying parameters on the upper surface of the model. The jets were used to alter the flowfield over the wing caused by leading-edge vortices. The natural location of vortex breakdown was shifted by three sets of PVC actuators strategically positioned on the model. This effect was intended to control the chordwise lift distribution over the wing by inducing both premature and delayed vortex breakdown, resulting in nose-up and nose-down pitch responses, respectively. A comparative analysis of this hingeless flow control concept was conducted in Texas A&M University's 3 × 4 ft low-speed wind tunnel and 2 × 3 ft water tunnel. Testing included force balance measurements, laser-fluorescene visualizations, surface flow visualizations, and schlieren shadowgraph visualizations. Visualization results show successful manipulation of the vortex breakdown locations over the delta-wing model. Force balance results also show that the aerodynamic characteristics of the delta wing were altered. Observations show changes primarily in pitching moment, with no detrimental changes in lift or drag.

Introduction

Background

SEVERAL recent efforts in the aerospace industry to investigate the effects of unconventional control schemes for future inhabited and uninhabited combat aircraft have taken place in response to the announcement of new design criteria for these aircraft. Recently, the U.S. Department of Defense fixed-wing vehicle initiative established cost, weight, agility, and survivability goals for combat air vehicles of the future. One approach in meeting these technical challenges is to reduce the size and number of conventional control surfaces, yet maintain maneuverability. Replacing the conventional moving control surfaces with hingeless devices in the form of innovative active flow control concepts could provide this reduction. Such applications could benefit combat aircraft with new airframes of lighter weight and less structural complexity due to the lack of numerous components needed for modern control schemes. In combat situations, these aircraft could experience enhanced maneuverability and survivability, as well as exhibit low-observability characteristics due to the absence of moving control surfaces. With the progress of current aerodynamics and controls research, the application of active flow control methods represents a promising and challenging alternative for the directional control and flight performance enhancement of tomorrow's combat fighter aircraft.

Active Flow Control

Passive flow control techniques use control devices that have a fixed geometry, and no energy input is necessary for their operation. Examples of passive flow control devices are riblets,[1] wing-tip devices,[2] vortex generators,[3] etc. These techniques are typically designed to perform optimally over a narrow range of flow conditions and cannot be altered as flow conditions change. Alternatively, active flow control techniques employ control devices that have actively modifiable configurations and need energy input to operate. In this sense, as flow conditions change, the geometry or system parameters of the control device can be altered to conform to the needs of the new environment. Examples of active flow control schemes include flow injection or suction,[4–6] actively deployable control surfaces such as trailing- or leading-edge flaps,[7] or deformable or pulsating boundaries.[8]

Another classification of flow control approaches is macroscale vs microscale flow control. Macroscale flow control involves large-scale, high-energy control schemes such as wing reconfiguration, airfoil shaping, and wing twist control.[9] Microscale flow control typically involves unsteady, small-scale, low-energy control inputs concentrated in high-receptivity regions of the flowfield.[10] The objective of the latter is to channel energy (internal, kinetic, and potential) already existing in the fluid into the desired form or direction. This process of microscale flow control is based on utilization of physical flow mechanisms that amplify introduced disturbances or control inputs, which stands apart from the "brute force" approach of macroscale control.

Pneumatic Vortex Control

Pneumatic vortex control (PVC) technology uses small jets of compressed gas, to inject energy into the flowfield about a solid body via slots or nozzles. These jets could create or manipulate vortical flows that generate forces that control the motion of the body. The application of PVC to modern combat aircraft is particularly attractive because these fighter configurations generate vortex-dominated flowfields. Vortices generated on aircraft wing leading edges and fuselage forebodies exhibit high-receptivity regions sensitive to perturbations. These vortical flowfields could be manipulated in such a fashion as to offer a powerful tool for aircraft control.

A large amount of previous research tested the manipulation of these vortex flowfields over various fighter configurations with a wide variety of pneumatic devices. These PVC actuators included jet nozzles,[11,12] slots,[13,14] and combinations of both,[15] which employ either blowing[16] or suction[17] as the primary fluid action. In reference to blowing actuators, several investigations have used unsteady or pulsed blowing[18,19] in contrast to steady blowing, to improve response times, effectiveness, and momentum efficiency of the actuators. Another novel concept to be included in this discussion of flow control actuators is known as the synthetic jet.[20] These

Received 1 May 2000; revision received 6 September 2001; accepted for publication 8 January 2002.

*Graduate Research Assistant, Aerospace Engineering Department. Student Member AIAA.
†Associate Professor, Aerospace Engineering Department. Associate Fellow AIAA.

devices have the capability to operate in both suction and blowing modes, through orifices or slots, neither adding nor ingesting mass from the surrounding fluid.[20]

Delta Wings

The design of delta-wing planforms dates back to the 1930s with the work of Alexander Lippisch and the pursuit of supersonic flight. Through the years, supersonic aircraft designs have implemented delta wings or derivatives of such to accomplish the performance necessary for high-speed flight. At these speeds, highly swept, thin wings with low aspect ratios minimize wave drag and maximize the performance for such fighter configurations. However, at subsonic speeds these slender-wing planforms operate very differently from the basic high-aspect ratio, straight wings commonly used at lower speeds. The performance of swept planforms outside the high-speed envelope is extremely important because most modern mission roles require subsonic operations a majority of the time. As a result, massive research has been conducted to understand the performance of slender wings in the low-speed regime and to adapt the delta wing for modern aircraft designs.[21,22]

Maneuverability Through Flow Control

Future fighter aircraft designs are expected to accomplish new standards of flight performance through the progress of active flow control research.[23,24] For supermaneuverability, fighters must operate routinely at high angles of attack. At these poststall conditions, maintaining lateral and longitudinal directional control poses a unique problem because conventional controls are somewhat ineffective at these attitudes and speeds. Flow control efforts have attempted to address the lateral control problem with the application of PVC devices on the forebody or forward fuselage of the aircraft.[25] In the area of longitudinal control of delta-wing aircraft, a specific phenomenon, known as vortex breakdown (VBD),[26,27] can significantly alter the aerodynamic performance of the wing. PVC devices have been extensively tested for the alleviation of VBD,[28] for lift enhancement at high angles of attack,[29] and as a means for controlling the strength and position of these vortices for aircraft pitch control.[17] For such pneumatic control research to be successful, attention must be paid to the energy requirements of the devices.

At low angles of attack α, the location of VBD usually occurs within the wake region downstream of the wing. With increasing α, the breakdown begins to migrate forward,[30] crossing the wing trailing edge and settling atop the wing surface. Once the VBD location is over the wing, the higher pressures of the "burst" reduce the suction levels created by the leading-edge vortices (LEV). A loss in vortex lift is then experienced, and the longitudinal stability of the planform may also be affected.[31] Aerodynamic studies have shown VBD to cause changes in the slopes of lift, drag, and pitching moments for slender planforms with highly swept leading edges.[32,33] Also, the magnitude of these VBD effects is dependent on the wing sweep angle Λ, and VBD is sensitive to adverse pressure gradients, such as that associated with the Kutta condition at the trailing edge of a planform.[34] Overall, VBD significantly modifies the global flowfield over swept wings and is, therefore, viewed by many researchers and the industry as an undesirable characteristic, performancewise.

Center of Pressure and VBD

Similar to the migration of vortex breakdown, the center of pressure over a delta wing also migrates forward with increasing angle of attack.[35] The c.p. for any wing planform is defined as the point on the chord of the wing through which the resultant forces act. For slender configurations, the forward migrations of both VBD and the c.p. are aerodynamically related (Fig. 1). VBD migration could be one of the driving mechanisms for the shifting of the c.p. location.

As mentioned earlier, the existence of VBD over a wing surface causes a reduction in vortex lift generation and a change in the total lift distribution in general. As VBD crosses over the wing trailing edge and moves forward, the LEV suction levels decrease from aft to apex with this forward migration. Similarly, the vortex lift distribution reduces from aft to apex, and the total lift distribution is also shifted forward. Therefore the change in the c.p. location can be caused by this change in planform lift distribution.

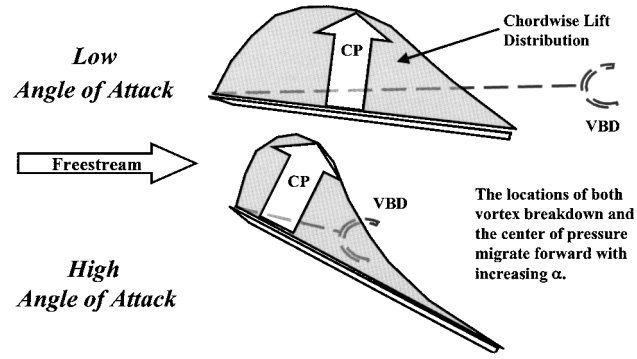

Fig. 1 Migration of VBD and c.p.

Aerodynamic Center and Center of Pressure

To examine the statement that a relationship exists between the migration of vortex breakdown and the c.p., measurements of each are necessary. Several surveys of VBD on delta-wing planforms have been recorded[36,37] as well as analytical methods for predicting the location of VBD.[38] However, little research has reported the behavior and position of the c.p. for this class of wings. Some observations have shown the c.p. to exist in a region near the geometric center of the delta wing, two-thirds of the root chord c_r from the apex, with forward migrations in the range of 0–5% c_r, for α less than 30 deg (Ref. 35). Again, this behavior is dependent on the model geometry and test conditions, which further necessitates measurement for a specific configuration.

Wind-tunnel testing has decreased the popularity of the c.p. Instead, in practice, the concept of the aerodynamic center (a.c.) is more frequently used.[31] The a.c. of a wing is defined as the point about which the moment coefficient is constant and independent of α (Refs. 31 and 38). As a stationary position, the a.c. is attractive for force and moment referencing as opposed to the c.p., which is constantly changing with lift. However, thin airfoil theory shows that these two points coincide on symmetrical airfoils.[38] When this result is applied to flat plate delta wings, which are inherently symmetric, the a.c. and c.p. are considered the same.

Hingeless Control Concept

In conjunction with the massive amount of aerodynamics research conducted to study the fundamental nature of LEV and VBD, other investigations have concentrated on the control of such flowfields. Much of this research has involved a wide variety of devices and modifications added to delta wings and other slender planforms.[22] Some of these devices include vortex flaps and plates,[39] tabbed vortex flaps,[40] apex flaps,[41] trailing-edge flaps,[42] and vertical fins.[43] Other tests consider modified wing leading-edge geometry such as shape,[44] the addition of slots and fences,[45] and contouring the wing apex.[46] The physical application of these devices to fighter aircraft would require additional components for operation and control, thus adding weight and complexity to the existing structure. This does not include the resulting poor observability qualities, or "stealth" characteristics, now being required in the designs of many fighters.

Alternatives to the aforementioned vortical control devices are hingeless control schemes, such as the PVC methods described earlier. The hingeless flow control concept designed for this investigation involves the strategic placement of PVC actuators on a delta-wing planform for the purpose of VBD manipulation and control (Fig. 2). These actuators operate in such a manner as to induce or delay the occurrence of VBD, thus shifting its position over the wing planform. As discussed earlier, research has shown that an adverse pressure gradient can induce VBD.[33,34] The adverse pressure gradient affects the ratio (azimuthal velocity)/(axial velocity) and, thus, the swirl angle, which has repeatedly been used as a criterion for

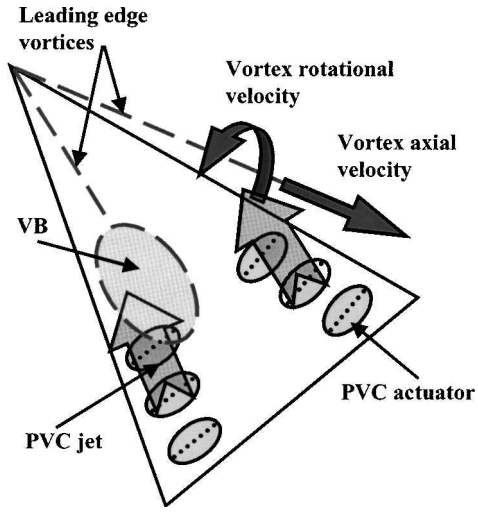

Fig. 2 Description of HFC concept.

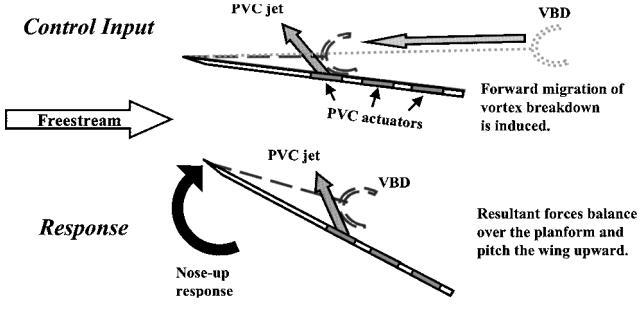

Fig. 3 Manipulation of VBD and resulting nose-up response.

VBD. Such an adverse pressure gradient could be introduced over the wing via PVC.

On this premise, if PVC actuators on a delta wing were to introduce jets of varying momentum into the vortex, thus inducing an adverse pressure gradient, a premature VBD event could be created near the point where the jets are introduced (Fig. 3). In turn, at a low α this PVC jet input could result in a nose-up pitch response due to the resulting forward migration of the c.p. A reverse process could also be initiated with the PVC jet orientation arranged to delay VBD at higher α. Studies of LEV behavior on delta wings undergoing ramp pitching[47] has lead to the investigation of VBD control during such maneuvers through the use of blowing.[48] These results encourage the flow control concept discussed here, which properly orchestrated should present a viable method for hingeless longitudinal control of a delta wing planform.

Experimental Equipment and Procedures

Hingeless Flow Control Model

The model used for this investigation was a delta-wing configuration and is referred to as the hingeless flow control (HFC) model. The HFC model was constructed from aluminum, as were all PVC actuator components and the mounting apparatus used for testing. The choice of a leading-edge sweep angle of 60 deg was based on current and future uninhabited combat aerial vehicle designs. This value of Λ also provided a wing geometry that allowed enough internal volume for the arrangement of PVC actuators across the planform. Figures 4 and 5a show the dimensions of the HFC model and a top view photograph taken with the model mounted inside the wind-tunnel test section, respectively. Further geometric parameters for the model are listed in Table 1. In Table 1, S is the wing planform area, t is its thickness, and γ is the leading edge bevel angle.

The HFC model has a relatively thick profile to provide internal space for mounting the PVC actuators and associated plumbing.

Table 1 Hingeless flow control model geometry

Parameter	Value
Λ, deg	60
S, in.^{2} (m^2)	113 (0.073)
AR	2.31
c_r, in. (m)	14 (0.356)
t/c_r	0.05
γ, deg	45

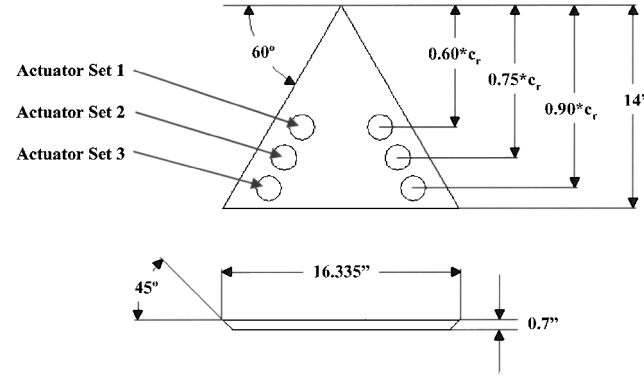

Fig. 4 HFC model geometry.

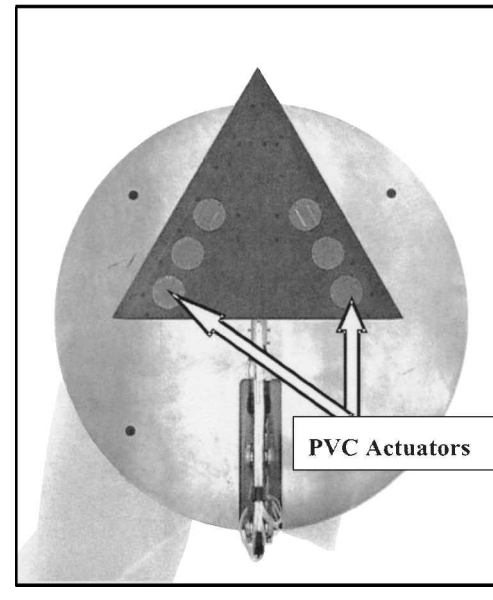

a)

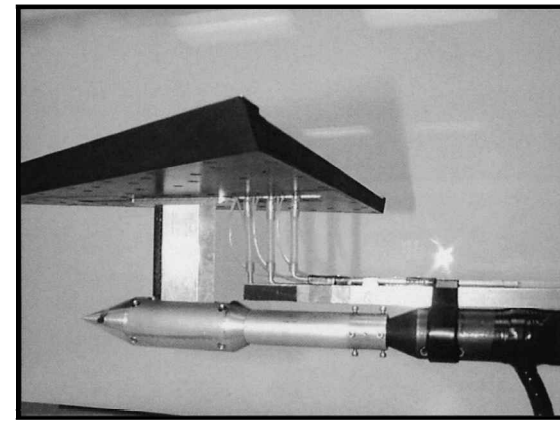

b)

Fig. 5 HFC model: a) top view from within the wind tunnel showing the actuators and b) delivery air lines and pneumatic coupling.

This provided a "clean" model with no unnecessary attachments to impose unwanted aerodynamic loads during testing. Delivery air was routed from the wind-tunnel mount into the HFC model through a specially designed pneumatic coupling (Fig. 5b). Metal tubing attached to the HFC model and the air lines from the sting mount were coupled together with soft rubber tubing, to allow flexibility during testing and to minimize interactions caused by pneumatic forces. This coupling was shrouded during tests. Pressurization tests, with the blowing orifices blocked, revealed negligible effect of the pneumatic couplings to the balance readings. However, even these negligible effects were accounted for by performing, before each wind-tunnel test, force and moment tares (no freestream), with the blowing set to a specific C_μ. These tares were taken for every single change in configuration, supply pressure, or C_μ.

The HFC model was also designed with a high degree of modularity. That is, components can be changed or replaced for various tests with neither major modifications to the existing structure, nor long turnaround times that may hamper the test schedule efficiency. Access to internal components can be achieved by simply removing the upper surface plate of the model.

The PVC actuators were simple in design, consisting of short cylindrical plenums or pressure chambers, open at one end, with plate covers that allowed pressurized air to escape through slots or orifices machined into these covers. The plenums fit inside the HFC model and had two ports machined into the circumference for incoming high-pressure delivery air and static pressure measurement, respectively (Fig. 6a). The actuator covers were thin plates, circular in shape, and machined with either a row of orifices along the diameter or a slot located on the circumference, (Figs. 6b and 6c). The covers fit flush with the upper surface of the HFC model through holes cut into the upper surface plate, and the two types could be removed or exchanged with ease.

The choice of actuator cover was based on the jet desired for a certain PVC configuration. The slotted actuator cover produced a wide, thin jet that blew parallel to the wing upper surface. The orifice actuator cover uses a row of holes to produce an overall wider jet at an inclination of 45 deg to the wing surface. The row of orifices was selected against a long thin slot due to the ease of fabrication. Also, the orifice row has an effective jet width the same as that from an equivalent slot, but the reduced exit area allows for higher jet velocities at lower mass flow rates. The actuator plenums

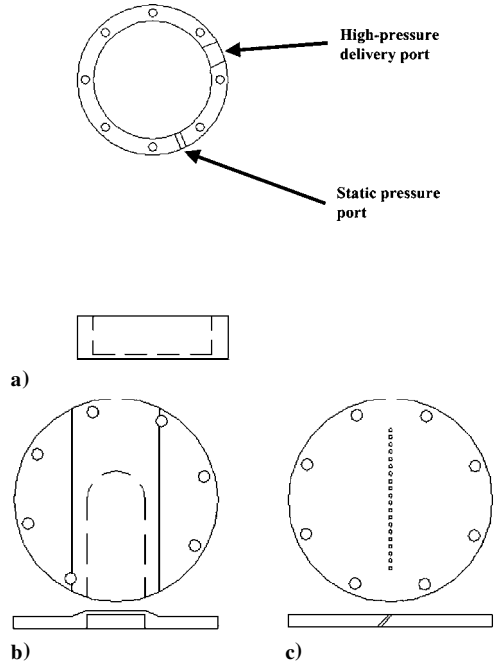

Fig. 6 PVC actuators: a) plenum, 1.75 in. diameter, 0.703 in.^{3} internal volume, and 0.5 in. thickness; b) surface jet cover, 0.0156 in.^{2} jet area, and 0.5 in. jet width; and c) 45-deg orifice cover, 0.0148 in.^{2} jet area, and 1.25 in. jet width.

Table 2 Actuator chordwise and spanwise locations

Actuator Set	x/c_r	y/s
1	0.60	0.564
2	0.75	0.651
3	0.90	0.685

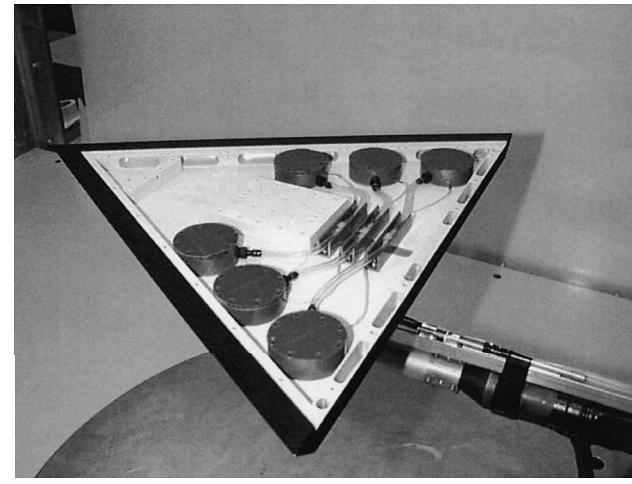

Fig. 7 Internal structure of HFC model (upper plate removed).

and covers were fastened together through an eight-hole-pattern of screws. This pattern allowed for the covers to be rotated and set at approximately 44-deg intervals. With the different combinations of pitch and azimuth settings, this small collection of actuator covers provided freedom to experiment with jets of varying orientation with respect to the HFC model.

A total of six PVC actuator plenums were fabricated and mounted to the HFC model. These were arranged in spanwise pairs at three different chordwise locations, as listed in Table 2, where x measures from the wing apex along the wing chord, y measures from the root chord of the wing perpendicular to it, c_r is the wing root chord, and s is the wing semispan. The locations were strategically selected based on the location of the LEV, derived from published research and examined through a brief wind-tunnel survey using a seven-hole pressure probe over the HFC model. The location of the LEV was found to be between 65 and 68% of the local semispan. The thickness of the leading-edge frames of the HFC model caused some restriction of the proposed locations for the actuators, as seen with the spanwise location of actuator set 1. Figure 7 shows a view of the HFC model with the upper surface plate removed, exposing the PVC actuators and plumbing.

Pneumatic Control System

To monitor the high-pressure air delivered to the HFC model, a pneumatic control system (PCS) was designed and constructed. Figure 8 shows a schematic of the PCS and a brief description of the components. The measurements taken with this setup were used to calculate a blowing coefficient $C\mu$. This parameter is widely used in flow control applications and provides a nondimensionalization of the blowing jet momentum for a pneumatic system. Equation (1) defines $C\mu$ as the ratio of the jet mass flow rate ($\dot{m}$) times the jet velocity V_j to freestream dynamic pressure q_∞ and model planform area S:

$$C\mu = \dot{m} \times V_j/(q_\infty \times S) \tag{1}$$

The pneumatic control system consists of 10 major components, as shown in Fig. 8. The first component was a high-pressure reservoir located at Texas A&M University's 3 × 4 ft low-speed wind-tunnel facility. A pressure regulator was connected to this reservoir and was set at a maximum of 60 psi to limit the pressure delivered to

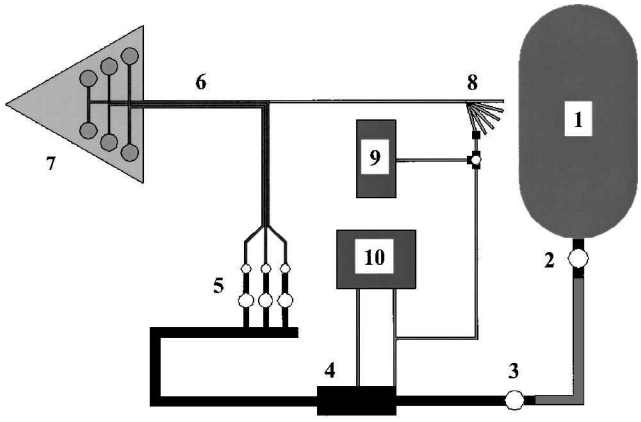

Fig. 8 PCS schematic: 1, high-pressure source; 2, pressure regulator; 3, main control valve; 4, venturi flow meter; 5, PVC delivery control valves; 6, PVC delivery pressure lines; 7, HFC model; 8, actuator static preesure lines; 9, high range manometer; and 10, low range manometer.

the PCS. The main control valve operated the PCS, allowing the pressurized air to enter a venturi flow meter. This flow metering device was fabricated and operated under British Standard design specifications and equations. Following the venturi are the main PVC control valves that direct air to each of the three sets of actuators via the three delivery pressure lines. These lines go up into the HFC model, through the coupling discussed earlier, and then branch off to left and right plenums for each actuator set.

From each actuator plenum, lines from the static pressure ports run out of the HFC model and are connected to a high-pressure range digital manometer. Here, plenum pressures are monitored by a Digitron Model 2083P digital manometer, with an accuracy of 0.1% of reading and a maximum range of 100 psi. With each plenum having its own pressure line, the left and right actuator pressures from one set could be compared for symmetrical blowing. A t valve was also connected to the digital manometer to allow measurement of the inlet pressure to the venturi flow meter. A low range manometer was used to measure the pressure drop across the flow meter inlet and throat section. A Dwyers water-filled manometer provided this measurement with an accuracy of ± 0.005 in. H_2O and a maximum range of 5 in. H_2O. These three pressure measurements contributed to the calculation of mass flow rate and jet velocity for the system.

Experimental Facilities

Tests were undertaken in the Aerospace Engineering 3×4 ft continuous wind tunnel. This tunnel has a turbulence intensity of approximately 0.3% at the test freestream velocity (20 m/s) and can achieve a maximum velocity of 50 m/s. The tunnel has active cooling and was maintained at a temperature of 22°C for the wind-tunnel tests. The freestream velocity was determined using a wall-mounted pitot tube. Differential pressure was measured using an Air Neotronics MP6KSR digital micromanometer. This manometer can resolve pressures down to 1 Pa. Manufacturer's calibration yielded an accuracy of better than 0.3% of full scale. The combination of the pitot probe and the manometer yielded a freestream measurement accuracy of 1%.

Tests were also conducted in the Aerospace Engineering 2×3 ft water tunnel. This tunnel has a glass test section 6 ft long and allows visual access for flowfield observation. A model mount mechanism allows both model pitch and yaw control during testing. The facility is capable of freestream velocities up to 0.9 m/s. Flow visualization is accomplished using a four-channel dye injection system. Also located in the facility is a 25 W argon-ion laser and associated optics used for flow visualization with fluorescent dye injection.

A six-component Aerolab sting balance was used for force and moment determination. The balance measures two normal and two side forces, as well as axial force and rolling moment. The two normal forces allow determination of pitching moment; similarly, the side forces yielded the yawing moment. Proof loads were applied to the balance in pure, as well as combined, loading configurations. From this, the accuracy of the balance is estimated at 0.5% of full scale for lift, drag, and pitching moment. This is within the accuracy limits prescribed by NASA for their balances.[49] Balance resolution is better than 2×10^{-4} of the measured coefficient on all channels. Through repeated data runs, repeatability of the balance for lift, drag, and pitching moment is estimated at $\Delta C_L = 0.0008$, $\Delta C_D = 0.0005$, and $\Delta C_m = 0.0008$. Model pitch and yaw is adjusted using dc motors connected through a potentiometer to a digital readout display. Model angel of attack can be set to within 0.05 deg. Force balance data as well as tunnel dynamic pressure were acquired using a personal computer equipped with a 16-bit A/D board. A data acquisition code, developed in-house by other researchers, was used for all force balance data acquisition.

Flow Visualizations

Off-surface visualization was used to characterize VBD manipulation. Tests were performed in the 2×3 ft water tunnel with a small 60-deg delta wing having a windward bevel of 45 deg, before the construction of the HFC model. Blowing over the wing surface was accomplished through attachment of small brass tubes, injecting water from one channel of the dye injection system. Fluorescent dye was injected from the wing apex and entrained by the LEV. When the 25-W argon-ion laser was used, a sheet of laser light was projected onto the wing surface and aligned parallel to the vortex core to allow the visualization of breakdown. Video of these tests was recorded and selected frames were used afterward for photographs.

Test Procedure

This investigation began with water-tunnel tests to survey different applications of blowing on a 60-deg delta wing. The freestream Reynolds number was maintained at $Re = 0.30 \times 10^6$ based on c_r. Jets varying in strength, location, and freestream orientation were examined for effects imposed on the LEV and the location of breakdown. The orientation of the jet was defined with respect to the freestream direction, in terms of two angles: its pitch angle and its azimuth angle, as defined in Fig. 9. Results gathered from these visualizations lead to the design of PVC actuators and their arrangement on the delta-wing model.

Next, the HFC model was designed with a priority given to the accomodation and operation of the PVC components. With a completed model and mounting apparatus, wind-tunnel tests were conducted to compare force measurements taken with and without PVC actuation. These tests were undertaken in the Aerospace Engineering 3×4 ft wind tunnel at $U = 20$ m/s and $Re = 0.48 \times 10^6$. The first wind-tunnel tests completed were for the case of no blowing actuation and represented the baseline configuration for this investigation. Following tests included blowing actuation and were divided into test "blocks," based on operated actuator set and jet orientation. Each test block was then subdivided into a series of tests for varying $C\mu$ values. A total of eight blocks were completed with five $C\mu$ tests for each. Angle of attack for all wind-tunnel tests ranged from 0 to 20 deg in 2-deg increments. All tests were conducted with a freestream velocity of 20 m/s and no sideslip angle. Baseline tests

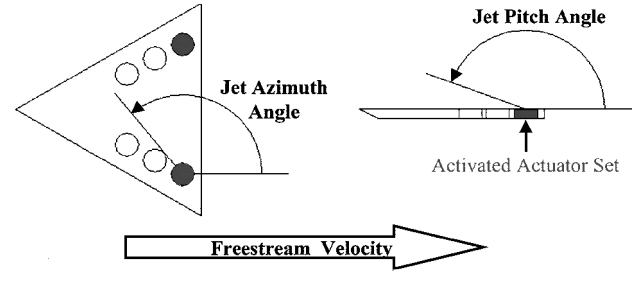

Fig. 9 Description of blowing configurations, where both jet azimuth and pitch angle are measured as shown.

included a static tare measurement to eliminate effects caused by the weight of the model and mounting apparatus. All blowing tests used a tare measurement with the PVC jets on, to eliminate jet momentum effects on the model.

Results and Discussion

Water-Tunnel Flow Visualization

Initial tests for this investigation consisted of an evaluation of PVC techniques that successfully manipulated the location of VBD. This was the first attempt at examining the hypothesis discussed earlier. To begin, jets were operated from a line of 10 small orifices drilled into the model and located directly underneath the path of the LEV. These orifices produced jets with a pitch angle of 135 deg at an azimuth angle of 158 deg, and were spaced longitudinally at $0.10^{*}c_r$ intervals. All tests were conducted with an α range of 0–12 deg and $C\mu$ levels up to 0.03. This initial attempt at PVC proved unsuccessful for instigating premature breakdown events, regardless of blowing rates. Although disruption of the vortical flowfield over the planform did occur, distinctive VBD occurrence was not witnessed. It was observed that once the orifice jets pierced the core of the vortex, the LEV structure altered its path around the jet and continued downstream. It was concluded that these jets emanating from a single point did not provide enough interaction with the axial and rotational flow of the LEV to produce instability capable of VBD. A second conclusion of these initial results was that the incidence angle between the jet and LEV was too large. It was assumed that a jet directed at a more shallow angle to the core may have a more destabilizing effect, thus leading to earlier VBD at low α.

Guided by the results, jets were placed on the delta-wing upper surface and directed forward into the LEV at low θ (the angle that the direction of the jet forms with the surface of the wing). Figures 10–13 show some of the results of the low θ PVC jets on the delta-wing vortex flow. All tests presented in Figs. 10–13 were conducted at an α of approximately 5 deg. Figures 10 ($C\mu = 0$) and 11 ($C\mu = 0.01$) show the results for an actuator located at the trailing edge and attached parallel to the wing surface. The jet was, thus, directed into the vortex from the trailing edge of the wing. Observations of this test showed good control for the onset of VBD. By increasing the $C\mu$ of the jet, the VBD location was pushed far upstream near the apex, totally eliminating the coherent LEV

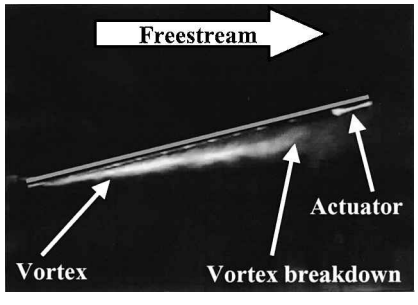

Fig. 10 Water-tunnel flow visualization with blowing off ($C\mu = 0$) and jet nozzle at the trailing edge.

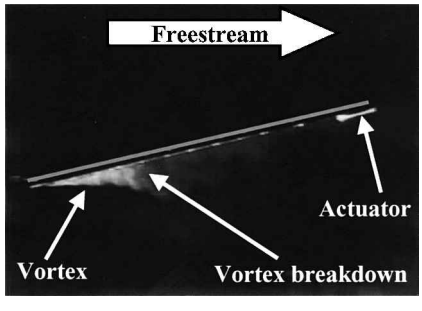

Fig. 11 Water-tunnel flow visualization, with blowing on from the trailing edge ($C\mu = 0.01$, $\theta = 0$ deg).

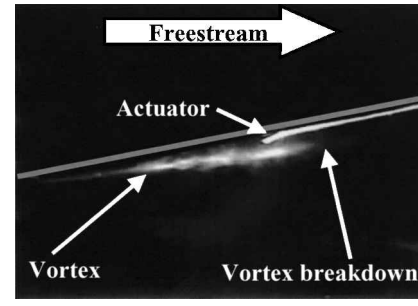

Fig. 12 Water-tunnel flow visualization, with blowing off ($C\mu = 0$) and jet nozzle at 60% chord.

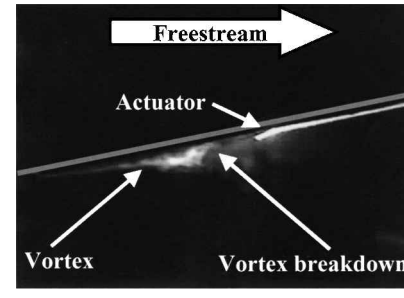

Fig. 13 Water-tunnel flow visualization, with blowing on at 60% chord ($C\mu = 0.001$, $\theta = 5$ deg).

structure. Although the blowing rates used for this large effect are rather high for physical applications ($C\mu = 0.01$), more localized control near the trailing edge of the wing was quite successful. Figures 12 ($C\mu = 0$) and 13 ($C\mu = 0.001$) used a similar PVC jet placed at $0.60^{*}c_r$ and blowing with a jet angle θ of 175 deg. This arrangement showed more localized shifts of VBD as compared to massive changes exhibited with the trailing-edge jet. The successful $C\mu$ values ($C\mu = 0.001$) for this PVC jet were much lower than the preceding tests. Tests at other angles of attack, between 0 and 12 deg, showed very similar behavior, except that, at angles less than 4 deg, it was harder to induce large migrations of the VBD position.

Aerodynamic Effects of PVC

All force balance tests were performed at $Re = 0.48 \times 10^6$ based on c_r. This value of Reynolds number is lower than other published investigations. However, previous research has shown that changes in the aerodynamic characteristics of delta wings at lower Reynolds number are minimal in comparison to those at high Reynolds number. For all experimental data to be accepted as valid, repeatability must be shown. Figure 14 shows repeated baseline tests for the HFC model, presenting lift data. Repeatability was seen to be very good. Similar repeatability tests were also performed for drag and pitching moment. Although these plots are not presented here for conciseness, they show equally good repeatability. (The reader can find these plots in Ref. 50.) Further comparison of these data was made to results presented by Wentz and Kohlman.[30] Wentz and Kohlman conducted a comprehensive force balance investigation of the effects of wing sweep on a range of planar delta wings, with Λ ranging from 45 to 80 deg. These results are often regarded as baseline data and have been used to verify numerous theoretical and computational methods. Figure 14 shows comparison of the baseline lift results for this investigation and those of Wentz and Kohlman[30] for a 60-deg delta wing. As can be seen, Fig. 14 shows very good agreement between the two sets of measurements.

Table 3 lists the block configurations tested with force balance measurements and the actuator sets and jet orientations for each. In blocks 10, 20, 30, and 40, the jets are directed upstream, whereas in blocks 50, 60, 70, and 80 they are directed downstream. The exact jet direction for each block is given in Table 3, in terms of its azimuthal and pitch angles, as graphically shown in Fig. 15. (The specific angle values in Fig. 15 correspond to block 10.)

Table 3 Summary of wind-tunnel test blocks and jet orientations

Test block	Actuator set	Jet azimuth angle, deg	Jet pitch angle, deg
10	3	158	135
20	2	158	135
30	1	158	135
40	3	150	180
50	2	−22	45
60	1	−22	45
70	3	−22	45
80	1	−30	0

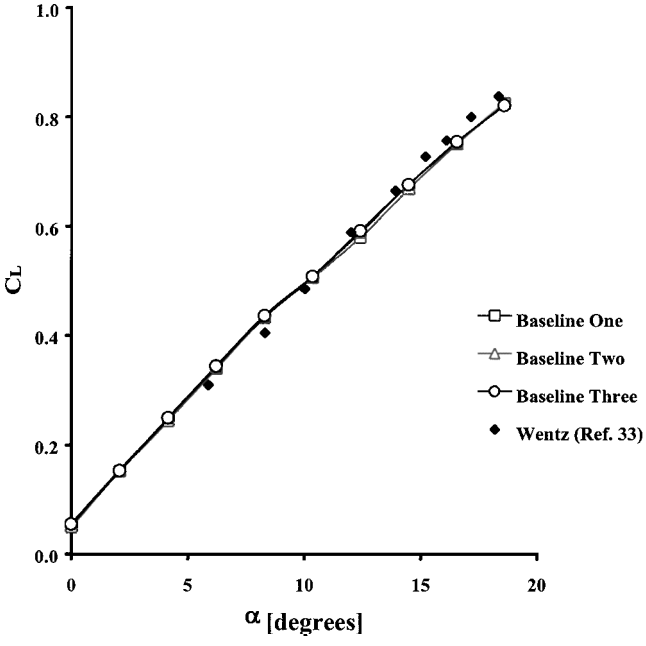

Fig. 14 Baseline results, lift coefficient vs angle of attack.

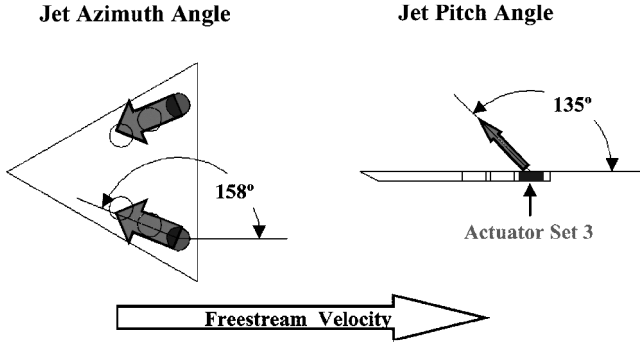

Fig. 15 Block 10 blowing configuration.

The plots for each block of tests consist of lift vs α, drag vs lift, pitching moment vs lift, and a.c. location vs lift, all in coefficient form. These plots included baseline results and the $C\mu$ series for each configuration. The pitching moment coefficient was calculated for a moment reference location at $0.40^{*}c_r$ and was nondimensionalized by c_r. Rae and Pope[36] present a description of the calculation for x_{ac}; however at low α, x_{ac} can simply be shown to be the difference between the moment reference location and dC_m/dC_L. Hence, x_{ac} plots are highly dependent on the slope of the C_m vs C_L curve and, therefore, related to longitudinal stability. The data for C_D and C_m vs C_L were plotted with zero-lift drag coefficients and zero-lift pitching moment coefficients removed to reduced tare and camber effects, respectively, imposed by the experimental setup.

The block 10 (configuration shown in Fig. 15) results show the most dramatic changes in aerodynamic performance of all of the configurations tested for PVC effects. An overall review of the data presented in Figs. 16–19 shows that change in the delta-wing flowfield is taking place and that the effects are global. Figure 16 shows that, with increasing $C\mu$, the lift of the wing steadily reduces. This reduction does not occur until the wing reaches an α above 4 deg, where the structure of the vortex begins to develop. From this observation, one can infer that this change in lift is related to changes in the vortex. The displacement in C_L blowing data from baseline data denotes a cambering effect. On regular wing planforms, the deployment of flaps is one example of cambering that changes the magnitude of lift while the slope, $dC_L/d\alpha$, remains the same. Also note that we attempted to reach "saturation" of the control effectiveness. In other words, we kept increasing the value of $C\mu$, until any additional increase of $C\mu$ did not cause additional change in the lift. As one can see from Fig. 16, increasing the value of $C\mu$ from 0.008 to 0.01 did not cause any additional change in the lift. This means that control saturation was reached.

In Fig. 17, the cambering effect is again present, this time with an upward shift in C_m signifying a decrease in negative pitching moment as a function of $C\mu$. The loss of lift and nose-down C_m corroborates the theory discussed earlier, where a reduction of the vortex lift component due to the onset of premature VBD would cause a change in longitudinal stability. The occurrence of pitch-up is also seen for the baseline wing at α of 10–14 deg, which compares with other research findings.[31] This is also the same α

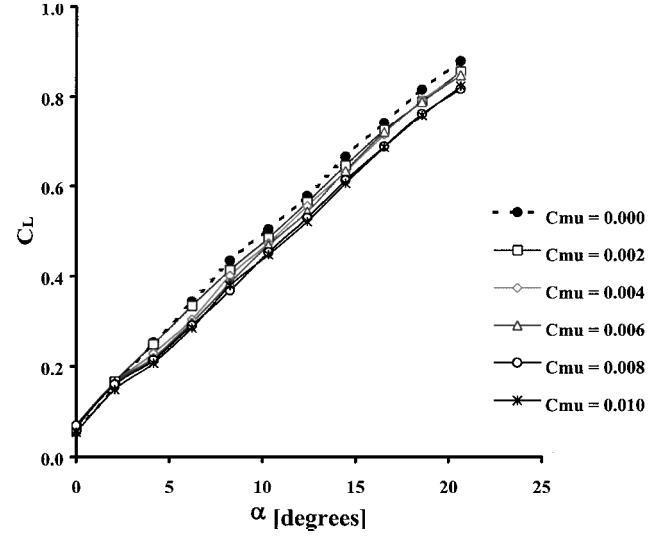

Fig. 16 Block 10, lift coefficient vs angle of attack.

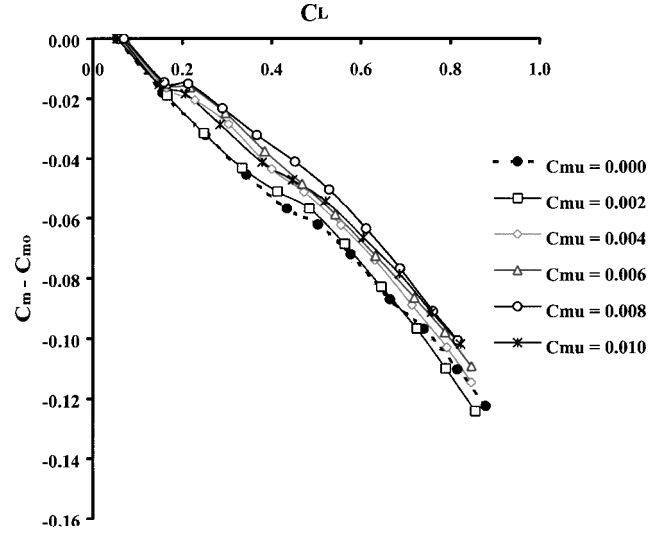

Fig. 17 Block 10, pitching moment coefficient vs lift coefficient.

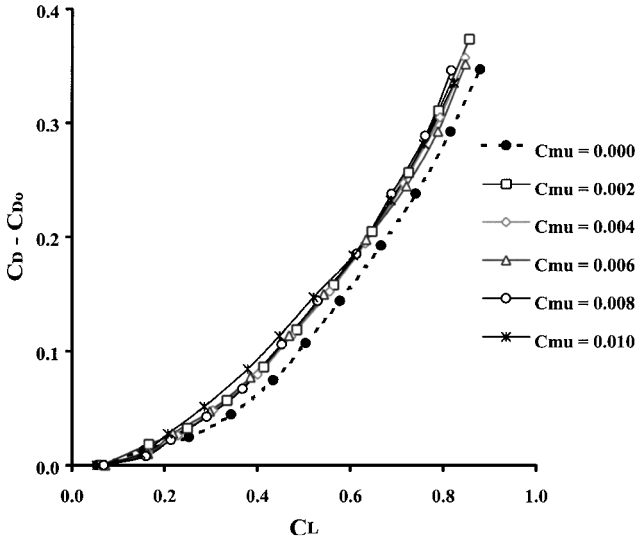

Fig. 18 Block 10, drag coefficient vs lift coefficient.

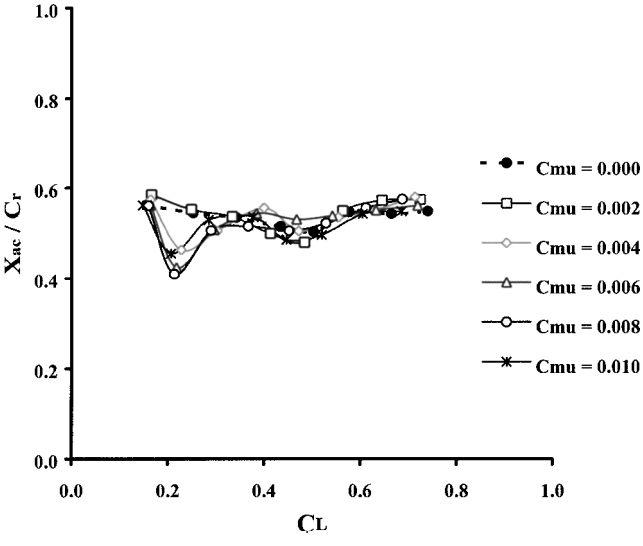

Fig. 19 Block 10, a.c. location vs lift coefficient.

range that VBD migrates across the wing trailing edge, by no coincidence. Pitch-up represents one of the effects caused by VBD over a planform, and its alleviation has been attempted through much research.[31] The result is a decrease in longitudinal stability, that is, a decrease in the slope, dC_m/dC_L, of the pitching moment curve and a reduced nose-down C_m, hence the term pitch-up. Figure 17 shows a trend of premature pitch-up at very low α with increasing $C\mu$. Not only does the pitch-up happen much earlier than the natural occurrence, but the magnitude of the change is far greater than that exhibited on the baseline wing.

Figure 18 shows an increase in drag for the block 10 configuration as a result of increasing blowing rates. This characteristic confirms that the manipulation of the LEV flowfield is creating global aerodynamic changes over the planform. A premature and large forward shift in the a.c. location is seen in Fig. 19. This was expected as a result of the changes witnessed in the C_m vs C_L data. Traub[51] showed that the a.c. on a delta wing moves forward with increasing α and described this as a result of trailing-edge influence. Kirkpatrick[52] went on to show that these trailing-edge effects, namely, the Kutta condition, influence the vortex lift more than the potential lift of the planform. As α increases, the vortex lift component of a slender wing becomes a greater contributor to the total lift, and therefore, the x_{ac} moves forward as trailing-edge effects increase. In Fig. 19, this characteristic is seen with the baseline results. A dip or "bucket" in the data occurs at the same C_L value as that for pitch-up with the

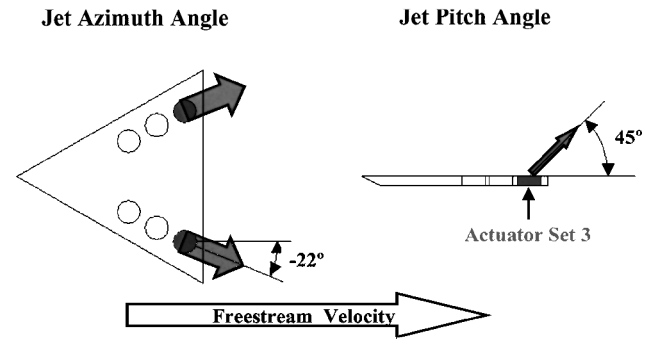

Fig. 20 Block 70 blowing configuration.

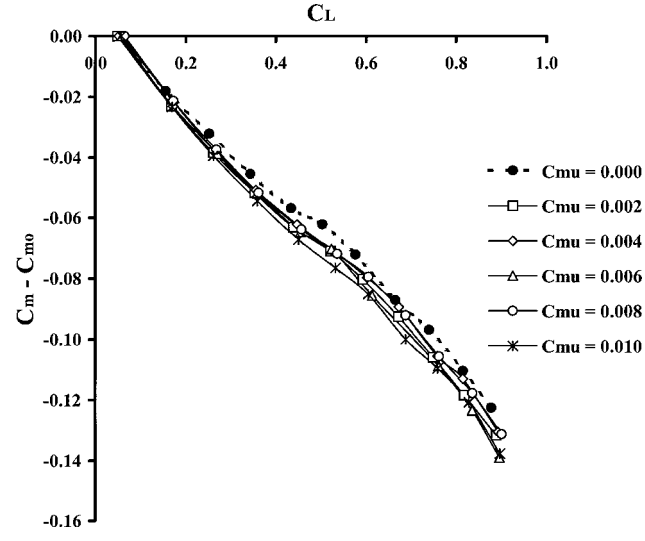

Fig. 21 Block 70, pitching moment coefficient vs lift coefficient.

baseline, and this is a good indicator of VBD effects. With increasing $C\mu$, the large forward shift in x_{ac} is created at low α, as expected with the early pitch-up seen in Fig. 17.

Blocks 50, 60, and 70 employed PVC jets with the same orientations, each from a different actuator set. Contrary to the block 10 tests already discussed, for these tests, the jet is directed in the downstream direction. Here, in the interest of space, we are only presenting some of the block 70 results. The results from all tests show that all trends observed in the force balance data are independent of chordwise jet location. The data for C_L, for all three tests, show a slight increase in lift as a function of $C\mu$. The pitching moment data for these three configurations show moderate nose-down changes. Figure 20 shows the blowing configuration for block 70, whereas Fig. 21 shows the variation of pitching moment as a function of the lift coefficient for various jet momentum coefficient values. Moderate nose-down moment control can be observed. Also, on viewing the data for the a.c. location, it was interesting to note that all trends exhibit independence of blowing rates.

Summary

An experimental investigation was conducted to investigate the use of VBD manipulation as an effective means for longitudinal control without the use of conventional hinged surfaces. This concept, referred to as HFC, employed the use of PVC actuators to instigate premature breakdown events or delay the onset of such, to alter chordwise load distributions over a 60-deg delta-wing planform. Several arrangements of actuators and jet combinations were tested. The objective was to produce nose-up and nose-down pitch responses through the use of strategically placed blowing jets. Tests were conducted in the Texas A&M University's 3 × 4 ft wind tunnel and 2 × 3 ft water tunnel in the form of force balance measurements and laser-induced fluorescene visualizations. Initial results showed that vortex manipulation was successful for blowing configurations

near the trailing edge, directed forward against the axial flow of the LEV. Further results and observations indicated changes in longitudinal characteristics for some of the configurations tested. Depending on the blowing configuration, both pitch-up and pitch-down moment control could be achieved. Successful delta-wing flow control was demonstrated, and new research approaches were identified for future work.

From the results and observations gathered, evidence suggests that the application of surface blowing on a delta-wing planform can alter the flowfield of the LEV in such a manner as to exhibit a form of longitudinal control. This form of control could be physically implemented on slender wings as an alternative or supplement to conventional moving, or hinged control surfaces. When ailerons or flaperons, are supplanted or augmented, HFC schemes could provide a lower observable planform for future inhabited and uninhabited combat aerial vehicles, thus improving mission performance and capability.

The experimental data presented in this investigation show successful manipulation of the VBD position over a 60-deg delta-wing planform. Measurements taken through force balance wind-tunnel tests confirm that these manipulations coincide with changes exhibited in the aerodynamic characteristics of the wing with emphasis on pitching moment. Moderate reduction in nose-down pitching moment was seen to occur, although further analysis is necessary to provide conclusive explanation of the flow physics responsible for these changes. This investigation did provide a comparative analysis of various blowing configurations that helped to identify successful schemes to be evaluated with further research.

Specifically, PVC jets located near the trailing-edge region of the wing, directed at a low incidence angles both parallel and opposite to the axial flow of the LEV, shows evidence as a successful means to HFC. The successful application of HFC schemes on delta-wing planforms is dependent on leading-edge sweep angle, which is related to the strength of the vortical flowfield, and PVC jet orientations, locations, and pneumatic blowing rates. With all of these issues considered, future research should show promising results that could lead to the employment of HFC in defense and civil aviation.

Acknowledgments

This work was supported by the Office of Naval Research, Contract N000014-97-1-0943, Allen Moshfegh Monitor, and by the Advanced Research Program of the State of Texas, Grant 95-39-RTD. The authors would also like to thank Richard Allen for his help with the experimental setups.

References

[1]Walsh, M. J., and Lindman, A. M., "Optimization and Application of Riblets for Turbulent Drag Reduction," AIAA Paper 84-0347, Jan. 1984.

[2]Traub, L. W., "Aerodynamic Effects of Delta Planform Tip Sails on Wing Performance," *Journal of Aircraft*, Vol. 31, No. 5, 1994, pp. 1156–1159.

[3]Wendt, B. J., "Measurements and Modeling of Flow Structure in the Wake of a Low Profile Wishbone Vortex Generator," NASA TM 106468, 1994.

[4]McCormick, S., and Gursul, I., "Effect of Shear-Layer Control on Leading-Edge Vortices," *Journal of Aircraft*, Vol. 33, No. 5, 1996, pp. 1170–1176.

[5]Gu, W., Robinson, O., and Rockwell, D., "Control of Vortices on a Delta Wing by Leading-Edge Injection," *AIAA Journal*, Vol. 31, No. 7, 1993, pp. 1177–1186.

[6]Maddalon, D. V., and Braslow, A. L., "Simulated-Airline-Service Flight Tests of Laminar-Flow Control with Perforated-Surface Suction," NASA TP 2296, March 1990.

[7]Nelson, C., Traub, L. W., and Rediniotis, O., "Progress Towards a Reduced Blade–Vortex Interaction Rotor," AIAA Paper 96-0150, Jan. 1996.

[8]Rediniotis, O., Lagoudas, D., Garner, L., and Wilson, L., "Development of a Spined Underwater Biomimetic Vehicle with SMA Actuators," Society of Photo-Optical Instrumentation Engineers 6th Annual International Symposium on Smart Structures and Materials, SPIE Paper 3667-22, March 1999.

[9]Chen, P. C., and Chopra, I., "A Feasibility Study to Build a Smart Rotor: Induced-Strain Actuation of Airfoil Twisting Using Piezoceramic Crystals," *Smart Structures and Intelligent Systems*, edited by N. W. Hagood, Proc. SPIE, Vol. 1917, 1993, pp. 238–254.

[10]McMichael, J. M., "Progress and Prospects for Active Flow Control Using Microfabricated Electro-Mechanical Systems (MEMS)," AIAA Paper 96-0306, Jan. 1996.

[11]Shih, C., and Ding, Z., "Trailing-Edge Jet Control of Leading-Edge Vortices of a Delta Wing," *AIAA Journal*, Vol. 34, No. 7, 1996, pp. 1447–1457.

[12]Iwanski, K., and O'Rourke, M., "F-15 Forebody Vortex Flow Control Using Jet Nozzle Blowing," AIAA Paper 95-1800, June 1995.

[13]O'Rourke, M., "Experimental Investigation of Slot Blowing for Yaw Control on a Generic Fighter Configuration with a Chined Forebody," AIAA Paper 95-1798, June 1995.

[14]Wood, N. J., and Roberts, L., "Control of Vortical Lift on Delta Wings by Tangential Leading-Edge Blowing," *Journal of Aircraft*, Vol. 25, No. 3, 1987, pp. 236–243.

[15]Lemay, S., Sewall, W., and Henderson, J., "Forebody Vortex Flow Control on the F-16C Using Tangential Slot and Jet Nozzle Blowing," AIAA Paper 92-0019, Jan. 1992.

[16]Fitzpatrick, K., Johari, H., and Olinger, D., "A Visual Study of Recessed Angled Spanwise Blowing Method on a Delta Wing," AIAA Paper 93-3246, April 1993.

[17]Maines, B., Moeller, B., and Rediniotis, O. K., "The Effects of Leading Edge Suction on Delta Wing Vortex Breakdown," AIAA Paper 99-0128, Jan. 1999.

[18]Moreira, J., and Johari, H., "Delta Wing Vortex Manipulation Using Pulsed and Steady Blowing During Ramp Pitching," AIAA Paper 95-1817, 1995.

[19]Meyer, J., and Seginer, A., "Effects of Periodic Spanwise Blowing on Delta-Wing Configuration Characteristics," *AIAA Journal*, Vol. 32, No. 4, 1994, pp. 708–715.

[20]Rediniotis, O. K., Ko, J., Yue, X., and Kurdila, A. J., "Synthetic Jets, Their Reduced-Order Flow Modeling and Applications to Flow Control," AIAA Paper 99-1000, Jan. 1999.

[21]Bertin, J. J., and Smith, M. L., *Aerodynamics for Engineers*, Prentice–Hall, Englewood Cliffs, NJ, 1989, pp. 282–288.

[22]Anderson, J. D., *Fundamentals of Aerodynamics*, McGraw–Hill, New York, 1991, pp. 356–365.

[23]Anglin, E. L., and Satran, D., "Effects of Spanwise Blowing on Two Fighter Airplane Configurations," *Journal of Aircraft*, Vol. 17, No. 12, 1980, pp. 883–889.

[24]Langan, K. J., and Samuels, J. J., "Effects of Wing Jet Blowing on the SHARC 55%-Scale Fighter Configuration," AIAA Paper 97-0039, Jan. 1997.

[25]Brandon, J. M., Simon, J. M., Owens, D. B., and Kiddy, J. S., "Free-Flight Investigation of Forebody Blowing for Stability and Control," AIAA Paper 96-3444, June 1996.

[26]Traub, L. W., "Prediction of Vortex Breakdown and Longitudinal Characteristics of Swept Slender Planforms," *Journal of Aircraft*, Vol. 34, No. 3, 1997, pp. 353–359.

[27]Vorobieff, P. V., and Rockwell, D. O., "Vortex Breakdown on Pitching Delta Wing: Control by Intermittent Trailing-Edge Blowing," *AIAA Journal*, Vol. 36, No. 4, 1998, pp. 585–589.

[28]Kuo, C. H., and Lu, N. Y, "Vortex Characteristics over a Delta Wing Subject to Transient Along-Core Blowing," *AIAA Journal*, Vol. 33, No. 12, 1995, pp. 2418–2420.

[29]Guillot, S., and Gutmark, E. J., "Lift Control of a Delta Wing by Jet Injection," AIAA Paper 99-0137, Jan. 1999.

[30]Wentz, W. H., and Kohlman, D. L., "Vortex Breakdown on Slender Sharp-Edged Wings," *Journal of Aircraft*, Vol. 8, No. 3, 1971, pp. 156–161.

[31]Rao, D. M., and Johnson, T. D., "Alleviation of the Subsonic Pitch-Up of Delta Wings," *Journal of Aircraft*, Vol. 20, No. 6, 1983, pp. 530–535.

[32]Earnshaw, P. B., and Lawford, J. A., "Low-Speed Wind-Tunnel Experiments on a Series of Sharp-Edged Delta Wings," Aeronautical Research Council, R&M 3424, London, May 1966.

[33]Lee, M., and Ho, C. M., "Vortex Dynamics of Delta Wings," *Frontiers in Experimental Fluid Mechanics*, Vol. 46, Lecture Notes in Engineering, Springer-Verlag, Berlin, 1989, pp. 365–427.

[34]Visser, K. D., and Nelson, R. C., "Measurements of Circulation and Vorticity in the Leading-Edge Vortex of a Delta Wing," *AIAA Journal*, Vol. 31, No. 1, 1993, pp. 104–111.

[35]Hoerner, S. F., and Borst, H. V., *Fluid-Dynamic Lift*, Hoerner Fluid Dynamics, Vancouver, Washington, 1985, Chap. 18.

[36]Rae, W. H., and Pope, A., *Low-Speed Wind Tunnel Testing*, Wiley, New York, 1984, pp. 242–247.

[37]Erickson, G. E., "Water-Tunnel Studies of Leading-Edge Vortices," *Journal of Aircraft*, Vol. 19, No. 6, 1982, pp. 442–448.

[38]Traub, L. W., "Simple Prediction Method for Location of Vortex Breakdown on Delta Wings," *Journal of Aircraft*, Vol. 33, No. 2, 1996, pp. 452–454.

[39]Rinoie, K., and Stollery, J. L., "Experimental Studies of Vortex Flaps and Vortex Plates," *Journal of Aircraft*, Vol. 31, No. 2, 1994, pp. 322–329.

[40]Hoffler, K. D., and Rao, D. M., "An Investigation of the Tabbed Vortex Flap," *Journal of Aircraft*, Vol. 22, No. 6, 1985, pp. 491–497.

[41]Klute, S. M., Rediniotis, O. K., and Telionis, D. P., "Flow Control over a Maneuvering Delta Wing at High Angles of Attack," *AIAA Journal*, Vol. 34, No. 4, 1996, pp. 662–668.

[42]Grantz, A. C., and Marchman, J. F., "Trailing Edge Flap Influence on Leading Edge Vortex Flap Aerodynamics," *Journal of Aircraft*, Vol. 20, No. 2, 1983, pp. 165–169.

[43]Reisenthel, P., Xie, W., Gursul, I., and Bettencourt, M., "Analysis of Fin Motion Induced Vortex Breakdown," AIAA Paper 99-0136, Jan. 1999.

[44]Bartlett, G. E., and Vidal, R. J., "Experimental Investigation of Influence of Edge Shape on the Aerodynamic Characteristics of Low Aspect Ratio Wings at Low Speeds," *Journal of the Aeronautical Sciences*, Vol. 22, No. 8, 1955, pp. 517–533.

[45]Rao, D. M., and Johnson, T. D., "Investigation of Delta Wing Leading-Edge Devices," *Journal of Aircraft*, Vol. 18, No. 3, 1981, pp. 161–167.

[46]Panton, R. L., "Effects of a Contoured Apex on Vortex Breakdown," *Journal of Aircraft*, Vol. 27, No. 3, 1990, pp. 285–288.

[47]Atta, R., and Rockwell, D., "Leading-Edge Vortices due to Low Reynolds Number Flow past a Pitching Delta Wing," *AIAA Journal*, Vol. 28, No. 6, 1990, pp. 995–1004.

[48]Johari, H., and Moreira, J., "Delta Wing Vortex Manipulation Using Pulsed and Steady Blowing During Ramp-Pitching," *Journal of Aircraft*, Vol. 33, No. 2, 1996, pp. 304–310.

[49]Guarino, J. F., "Calibration and Evaluation of Multicomponent Strain-Gage Balances," NASA Interlaboratory Force Measurements Group Meeting, Jet Propulsion Lab., Pasadena, CA, April 1964.

[50]Moeller, E. B., "Hingeless Flow Control Over Delta Wing Planforms," M.S. Thesis, Aerospace Engineering Dept., Texas A&M Univ., College Station, TX, Aug. 1999.

[51]Traub, L. W., "Effects of Spanwise Camber on Delta Wing Aerodynamics: An Experimental and Theoretical Investigation," Ph.D. Dissertation, Dept. of Aerospace Engineering, Texas A&M Univ., College Station, TX, May 1999.

[52]Kirkpatrick, D. L. I., "Investigation of the Normal Force Characteristics of Slender Delta Wings with Various Rhombic Cross-Sections in Subsonic Conical Flow," Aeronautical Research Council, Rept. C.P. 922, London, 1967.